IEEE Access
Multidisciplinary | Rapid Review | Open Access Journal

Received March 20, 2021, accepted April 8, 2021, date of publication April 16, 2021, date of current version April 30, 2021.

Digital Object Identifier 10.1109/ACCESS.2021.3073671

Method of Postures Selection for Industrial Robot Joint Stiffness Identification

YIRAN ZHANG[1,2], KAI GUO[1,2], (Member, IEEE), JIE SUN[1,2], AND YUJING SUN[3]

[1]Key Laboratory of High-efficiency and Clean Mechanical Manufacture, National Demonstration Center for Experimental Mechanical Engineering Education, School of Mechanical Engineering, Shandong University, Jinan 250061, China
[2]Research Center for Aeronautical Component Manufacturing Technology and Equipment, Shandong University, Jinan 250061, China
[3]School of Mechanical and Automotive Engineering, Qilu University of Technology, Jinan 250353, China

Corresponding author: Kai Guo (kaiguo@sdu.edu.cn)

This work was supported in part by the National Natural Science Foundation of China under Grant 51975335 and Grant 51605256; in part by the Key Research and Development Program of Shandong Province under Grant 2019GGX104008, Grant 2019GGX104006, and Grant 2019JZZY020318; and in part by the Key Laboratory of High-Efficiency and Clean Mechanical Manufacture at Shandong University, Ministry of Education under Grant 10000086393113.

ABSTRACT Industrial robots are being widely applied to machining operations, and are gradually becoming competitive with traditional CNC machining centers. Obtaining accurate stiffness values of robotic joints is the foundation for deflections compensation in case of large cutting forces. A number of factors influence the accuracy of joint stiffness identification, especially robotic posture. This paper proposes a robust and accurate method for selecting suitable postures in the joint stiffness identification. The identification process of the joint stiffness matrix is presented, an index considering both the dexterity and the condition number of the observation matrix is then developed, and the procedure for postures selection based on it is provided. The results of simulations and experiments show that the proposed method is more robust and accurate than classical method.

INDEX TERMS Joint stiffness identification, postures selection, observation matrix, condition number, dexterity.

I. INTRODUCTION

Serial robots with six degrees of freedom (6 DoFs) are used in a variety of machining applications, such as milling [1], [2], drilling [3], [4], and boring [5]. These machining processes feature large forces that can lead to an inaccurate global pose of the robot. To improve the performance of robots in machining, one solution involves compensating for deflections to ensure an accurate position and orientation of the end-effector based on the Cartesian stiffness matrix of the robot. Deblaise *et al.* [6] proposed the Virtual Joint Method (VJM) to model the stiffness of Parallel Kinematic Machines (PKMs), and this method is suitable for modeling robotic stiffness as well. The VJM regards links as rigid, and uses torsional springs to model the joints. A 6×6 stiffness matrix can be obtained based on the VJM for serial robots with 6 DoFs. It features a small number of nodes in its calculation [7]. Using the VJM, Salisbury [8] reported the stiffness matrix-based relationship between Cartesian space and that of the joints. Chen and Kao [9] proposed the conservative congruence transformation (CCT) to develop Salisbury's theory. Therefore, we can pay attention to the robot joint stiffness identification to form the robot joint stiffness matrix, then calculate the robot Cartesian stiffness matrix based on the robot stiffness models mentioned above.

To identify stiffness in robotic joints, Abele *et al.* [10] used different configurations of joints in the workspace, applied load on the end-effector, and measured the corresponding displacements. Then some interpolations have been used in the identification process. The most commonly used approach to joint stiffness identification is as follows: (1) A kinematic index– dexterity is used to select the configurations of robotic joints. (2) An external wrench (force and moment) is applied to the loading point of the end-effector, and the load is changed within the rated range of the robot. (3) The displacements (translations and rotations) of the end-effector are measured. (4) The stiffness values of the robot's joints are identified based on the stiffness model and linear least-squares theory.

Dexterity is a useful index for a robot system as it indicates the distance to singularities. Dumas *et al.* [11] noted that good dexterity is required for the joint stiffness identification

The associate editor coordinating the review of this manuscript and approving it for publication was Vlad Diaconita.

procedure to converge. Therefore, the zones of the robot's workspace and the joint space in which it has good dexterity need to be selected before tests. This is to say that not all postures are suitable for joint stiffness identification. Furthermore, with regard to the influence of the additional matrix K_C in Chen's robot stiffness model, postures of the robot with negligibly small values of K_C with respect to K_θ can be selected and simplified for the stiffness model of the robot. Moreover, the robot's Cartesian stiffness matrix depends on its posture [12]. Various postures lead to different stiffness characteristics of the end-effector, which can influence the accuracy of joint stiffness identification. Thus, selecting suitable robotic postures is significant for joint stiffness identification.

The most common method for selecting suitable robotic postures considers both dexterity and the influence of the additional matrix K_C. Postures with higher dexterity and a lower effect of K_C are usually selected for joint stiffness identification tests. The second and third joints of the robot are the most influential for the movements of its end-effector, Dumas *et al.* [11], [13] thus examined the relevant zones by setting the angle of the first joint to null, and that of the fourth, fifth, and sixth joints to 45°. They quantified the influence of the additional matrix K_C in those zones based on the relative deviations in the translational displacement and rotational displacement. The zones of joint space where the robot had good dexterity, and small values of relative deviations were hence selected. By comparing the zones of joint space, they found that the configurations for which the influence of K_C on K is the maximum also involve poor dexterity, i.e., close to the singularity [13]. Dumas *et al.* [11] also noted that the stiffness of all joints can been accurately identified if they are stressed substantially at least once in all tests. However, they did not provide detailed illustrations for the procedure to ensure this criterion. Yang *et al.* [14] used the indices of errors in the relative position and orientation to characterize errors in the identified joint stiffness and their effect on the predicted deflections. Suitable robot postures can be selected based on these indices. Unlike the theoretical basis for this research, Cen and Melkote [15] used a small static load to minimize the effect of K_C, and selected 15 joint configurations of the robot to cover all its spaces of motion and identify joint stiffness. Alici and Shirinzadeh [16] proposed a method to identify and characterize joint stiffness using Chen's stiffness model. They considered the influence of the additional matrix K_C and chose 20 postures in the robot's workspace. In summary, the second and third joints of the robot are the major objects of research when choosing robotic postures, and an appropriate zone of joint space can be selected based on the various indices.

Lehmann *et al.* [17] introduced an approach that involved clamping the robot's end-effector to a rigid environment and mounting a force/torque sensor between the end-effector and the fixture. Joint stiffness and other parameters were then calculated based on the robot controller and sensor data. This clamping solution was first proposed by Bennett *et al.* for kinematic calibration [18]. Jubien *et al.* [19] have also used it for identifying joint stiffness. Notably, this method does not require a force/torque sensor.

This paper proposes a method to improve the accuracy of identification of stiffness in robotic joints. This work makes one contribution to the literature: it is the first time to illustrate the relationship between the condition number of the observation matrix and the accuracy of the joint stiffness identification. On this basis, a new index taking into account both the dexterity and the condition number of the observation matrix is presented to search for suitable joint configurations. The robustness and accuracy of the method were verified by the theoretical analysis, simulations and experiments.

The remainder of this paper is organized as follows: In Section II, we detail the identification procedure to obtain the joint stiffness matrix. A novel index considering both the dexterity and the condition number of the observation matrix is presented in Section III, and Section IV is devoted to validating the robustness and accuracy of the proposed method through numerical simulations and experiments. Section V summarizes the conclusions of this study.

II. JOINT STIFFNESS MATRIX IDENTIFICATION

In this paper, we consider a non-damping system, assume that the robot's links are rigid, and the joints are regarded as torsion springs. A schematic of the stiffness model of the robot is provided in Fig. 1, and a diagonal joint stiffness matrix K_θ can be given by:

$$K_\theta = \begin{bmatrix} k_{\theta_1} & 0 & 0 & 0 & 0 & 0 \\ 0 & k_{\theta_2} & 0 & 0 & 0 & 0 \\ 0 & 0 & k_{\theta_3} & 0 & 0 & 0 \\ 0 & 0 & 0 & k_{\theta_4} & 0 & 0 \\ 0 & 0 & 0 & 0 & k_{\theta_5} & 0 \\ 0 & 0 & 0 & 0 & 0 & k_{\theta_6} \end{bmatrix}$$

Owing to the particular structure of the series connection, stiffness is not a fixed value in Cartesian space. It is a posture-dependent matrix, also called the Cartesian stiffness matrix K. The relationship between the external wrench vector $\boldsymbol{W}$ applied to the end-effector and the six-dimensional displacement vector $\boldsymbol{\Delta}$ is termed as:

$$\begin{aligned} \boldsymbol{W} &= [\boldsymbol{F} \quad \boldsymbol{M}] = [f_x \quad f_y \quad f_z \quad m_x \quad m_y \quad m_z]^T \\ \boldsymbol{\Delta} &= [\delta x \quad \delta y \quad \delta z \quad \delta\alpha_x \quad \delta\alpha_y \quad \delta\alpha_z]^T \\ \boldsymbol{W} &= K\boldsymbol{\Delta} \end{aligned} \tag{1}$$

where the force vector $\boldsymbol{F}$ is composed of the three elements $[f_x \quad f_y \quad f_z]^T$, and the moment vector $\boldsymbol{M}$ is composed of the other three elements $[m_x \quad m_y \quad m_z]^T$. Salisbury's model is used for joint stiffness identification, and it is expressed as:

$$K = J^{-T} K_\theta J^{-1} \tag{2}$$

Identifying the joint stiffness that means obtaining the values of each element in the diagonal joint stiffness matrix K_θ is the primary subject of this study. The detailed process of identification of the joint stiffness matrix K_θ is indicated in Fig. 2.

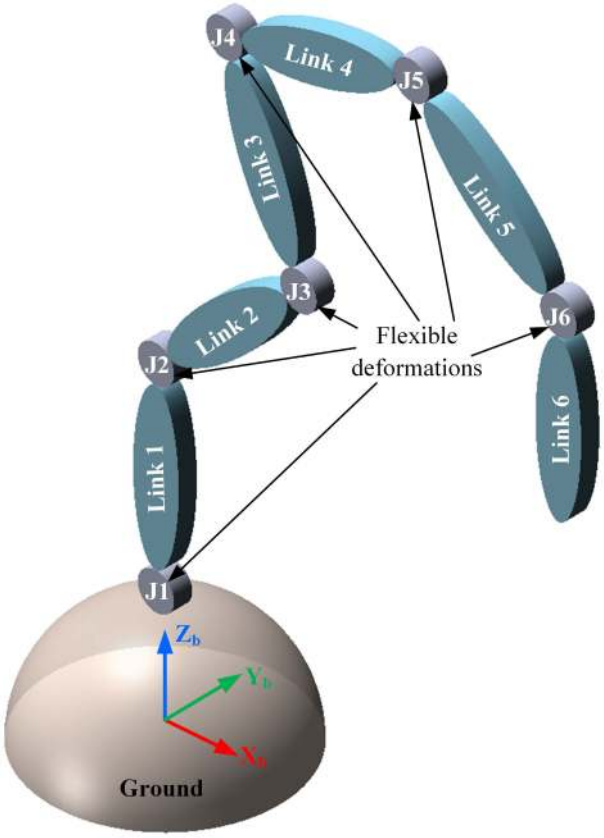

FIGURE 1. Schematic of the robotic stiffness model.

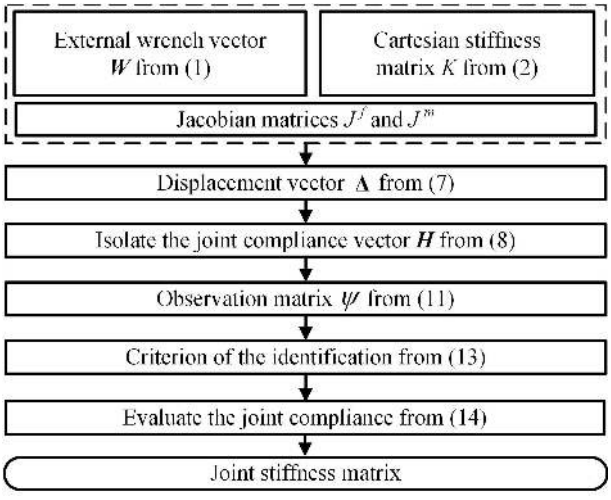

FIGURE 2. Detailed identification process of the joint stiffness matrix.

Combining Eq. (1) and Eq. (2), the new equation can be termed as:

$$\boldsymbol{\Delta} = JK_{\theta}^{-1}J^{T}\boldsymbol{W} \tag{3}$$

Owing to the different positions of the loading and measuring points, two types of Jacobian matrices are used. J^f is the Jacobian matrix representing the loading point and J^m is one representing the measuring point. Hence, the torque vector $\boldsymbol{\Gamma}$ acted on each joint can be termed as:

$$\begin{aligned}\boldsymbol{\Gamma} &= (J^f)^T\boldsymbol{W}\\ \boldsymbol{\Gamma} &= [\tau_1 \quad \tau_2 \quad \tau_3 \quad \tau_4 \quad \tau_5 \quad \tau_6]^T\end{aligned} \tag{4}$$

Besides, the torque vector $\boldsymbol{\Gamma}$ can also be expressed as:

$$\boldsymbol{\Gamma} = K_{\theta}\boldsymbol{\Delta q} \tag{5}$$

where $\boldsymbol{\Delta q} = [\Delta q_1 \quad \Delta q_2 \quad \Delta q_3 \quad \Delta q_4 \quad \Delta q_5 \quad \Delta q_6]^T$ represents the joint deflection vector.

What's more, the displacement vector $\boldsymbol{\Delta}$ of the end-effector can be expressed as:

$$\boldsymbol{\Delta} = J^m\boldsymbol{\Delta q} \tag{6}$$

Then combining Eqs. (4)-(6), Eq. (3) can be rewritten as:

$$\boldsymbol{\Delta} = J^m K_{\theta}^{-1}(J^f)^T\boldsymbol{W} \tag{7}$$

Let the joint compliance vector $\boldsymbol{H}$, namely:

$$\boldsymbol{H} = [k_{\theta_1}^{-1} \quad k_{\theta_2}^{-1} \quad k_{\theta_3}^{-1} \quad k_{\theta_4}^{-1} \quad k_{\theta_5}^{-1} \quad k_{\theta_6}^{-1}]^T \tag{8}$$

where $k_{\theta_i}^{-1}$ $(i = 1, 2, \ldots, 6)$ is the inverse of the ith joint stiffness value. Then Eq. (7) can be rewritten as:

$$\boldsymbol{\Delta} = \begin{bmatrix} \sum_{j=1}^{6}(k_{\theta_j}^{-1}J_{1j}^m\sum_{i=1}^{6}J_{ij}^f w_i) \\ \sum_{j=1}^{6}(k_{\theta_j}^{-1}J_{2j}^m\sum_{i=1}^{6}J_{ij}^f w_i) \\ \sum_{j=1}^{6}(k_{\theta_j}^{-1}J_{3j}^m\sum_{i=1}^{6}J_{ij}^f w_i) \\ \sum_{j=1}^{6}(k_{\theta_j}^{-1}J_{4j}^m\sum_{i=1}^{6}J_{ij}^f w_i) \\ \sum_{j=1}^{6}(k_{\theta_j}^{-1}J_{5j}^m\sum_{i=1}^{6}J_{ij}^f w_i) \\ \sum_{j=1}^{6}(k_{\theta_j}^{-1}J_{6j}^m\sum_{i=1}^{6}J_{ij}^f w_i) \end{bmatrix} \tag{9}$$

where w_i $(i = 1, 2, \ldots, 6)$ is the ith variable of the wrench vector $\boldsymbol{W}$. Besides, through isolating the joint compliance vector $\boldsymbol{H}$ in Eq. (9), it turns out that:

$$\Psi\boldsymbol{H} = \boldsymbol{\Delta} \tag{10}$$

where Ψ is a 6×6 matrix as:

$$\Psi = \begin{bmatrix} J_{11}^m\sum_{i=1}^{6}J_{i1}^f w_i & \cdots & J_{16}^m\sum_{i=1}^{6}J_{i6}^f w_i \\ J_{21}^m\sum_{i=1}^{6}J_{i1}^f w_i & \cdots & J_{26}^m\sum_{i=1}^{6}J_{i6}^f w_i \\ \vdots & \ddots & \vdots \\ J_{61}^m\sum_{i=1}^{6}J_{i1}^f w_i & \cdots & J_{66}^m\sum_{i=1}^{6}J_{i6}^f w_i \end{bmatrix} \tag{11}$$

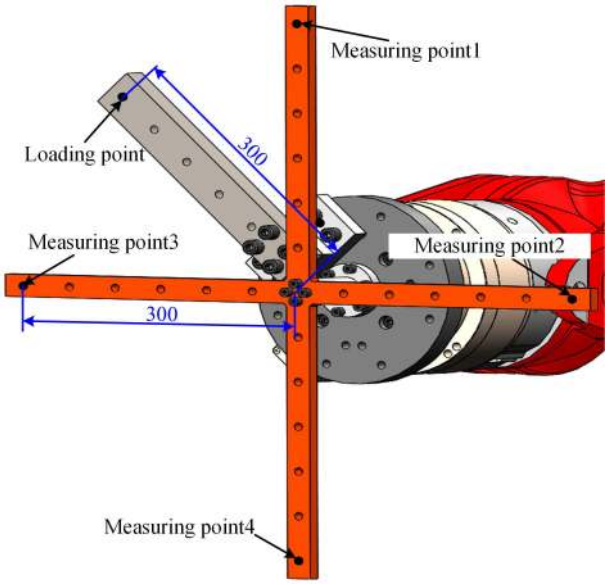

FIGURE 3. Schematic of the measuring/loading points (mm).

A six-dimensional square matrix is thus obtained, and is called the observation matrix. Rewriting Eq. (10), and the new equation can be termed as:

$$\boldsymbol{H} = \Psi^{-1}\boldsymbol{\Delta} \tag{12}$$

It is usually unrealistic to find an exact joint compliance vector $\boldsymbol{H}$ that satisfies all $6n$ equations (n is the number of tests, Ψ is a $6n\times6$ matrix). In this case, joint stiffness can be calculated by minimizing the error ε based on the Euclidean norm:

$$\text{minimize} \quad \varepsilon = \frac{1}{2}\|\Psi\boldsymbol{H} - \boldsymbol{\Delta}\|^2 \tag{13}$$

The joint compliance vector $\boldsymbol{H}$ can be used to minimize this norm of the approximation error of the system:

$$\boldsymbol{H} = (\Psi^T\Psi)^{-1}\Psi^T\boldsymbol{\Delta} = \Psi^l\boldsymbol{\Delta} \tag{14}$$

where Ψ^l is the generalized inverse of Ψ. Based on its definition, the stiffness values of each joint can be identified by solving the joint compliance vector $\boldsymbol{H}$ and the diagonal joint stiffness matrix K_θ can be calculated directly.

The traditional rope-mass loading method was used in the joint stiffness identification tests to impose the external wrench. As shown in Fig. 3, the corresponding displacements of the end-effector at the four measuring points were noted by a laser tracker and the external wrench was applied to the loading point. The exact joint stiffness values were identified based on the experimental data and the process mentioned above.

III. METHOD FOR POSTURES SELECTION

A. CONDITION NUMBER OF OBSERVATION MATRIX

The influence of the condition number of the observation matrix on the accuracy of the joint stiffness identification process is examined in this section. Let two matrix Ω and Λ, namely:

$$\Omega = \Psi^T\Psi$$
$$\Lambda = \Psi^T\boldsymbol{\Delta}$$

Substitute them into Eq. (14), we have:

$$\Omega\boldsymbol{H} = \Lambda \tag{15}$$

It becomes a linear least-squares problem. Finding a way to identify a more accurate joint compliance vector $\boldsymbol{H}$ is the core of research. Assuming that $\delta\Omega$, $\delta\boldsymbol{H}$ and $\delta\Lambda$ are the errors of Ω, $\boldsymbol{H}$ and Λ, respectively. Therefore, the relative error coefficients of Ω, $\boldsymbol{H}$ and Λ can be termed as $\frac{\|\delta\Omega\|}{\|\Omega\|}$, $\frac{\|\delta\boldsymbol{H}\|}{\|\boldsymbol{H}\|}$ and $\frac{\|\delta\Lambda\|}{\|\Lambda\|}$, respectively. In the joint stiffness identification process, $\frac{\|\delta\Omega\|}{\|\Omega\|}$ and $\frac{\|\delta\Lambda\|}{\|\Lambda\|}$ are supposed not to change.

For the error of Ω, it satisfies:

$$\|-\Omega^{-1}\delta\Omega\| = \|\Omega^{-1}\delta\Omega\| < 1$$

and the following equation can be termed as:

$$\begin{aligned}\|(I+\Omega^{-1}\delta\Omega)^{-1}\| &\le \frac{1}{1-\|\Omega^{-1}\delta\Omega\|}\\ &\le \frac{1}{1-\|\Omega^{-1}\|\|\delta\Omega\|}\end{aligned}$$

For Eq. (15), considering the errors of each term, the new equation can be termed as:

$$(\Omega+\delta\Omega)(\boldsymbol{H}+\delta\boldsymbol{H}) = (\Lambda+\delta\Lambda) \tag{16}$$

Based on Eq. (16), $\delta\boldsymbol{H}$ can be termed as:

$$\begin{aligned}\delta\boldsymbol{H} &= (\Omega+\delta\Omega)^{-1}[(\Lambda+\delta\Lambda)-\boldsymbol{H}(\Omega+\delta\Omega)]\\ &= (I+\Omega^{-1}\delta\Omega)^{-1}\Omega^{-1}(\delta\Lambda-\delta\Omega\boldsymbol{H})\end{aligned} \tag{17}$$

The norm of $\delta\boldsymbol{H}$ can be termed as:

$$\begin{aligned}\|\delta\boldsymbol{H}\| &= \|(I+\Omega^{-1}\delta\Omega)^{-1}\Omega^{-1}(\delta\Lambda-\delta\Omega\boldsymbol{H})\|\\ &\le \frac{\|\Omega^{-1}\|}{1-\|\Omega^{-1}\|\|\delta\Omega\|}(\|\delta\Lambda\|+\|\delta\Omega\|\|\boldsymbol{H}\|)\\ &= \frac{\|\Omega^{-1}\|\|\Omega\|\|\boldsymbol{H}\|}{1-\|\Omega^{-1}\|\|\delta\Omega\|}(\frac{\|\delta\Lambda\|}{\|\Omega\|\|\boldsymbol{H}\|}+\frac{\|\delta\Omega\|}{\|\Omega\|})\end{aligned} \tag{18}$$

We focus on the relative error coefficient $\frac{\|\delta\boldsymbol{H}\|}{\|\boldsymbol{H}\|}$, and Eq. (19) can be used to indicate this index:

$$\begin{aligned}\frac{\|\delta\boldsymbol{H}\|}{\|\boldsymbol{H}\|} &= \frac{\|\Omega^{-1}\|\|\Omega\|}{1-\|\Omega^{-1}\|\|\delta\Omega\|}(\frac{\|\delta\Lambda\|}{\|\Omega\|\|\boldsymbol{H}\|}+\frac{\|\delta\Omega\|}{\|\Omega\|})\\ &\le \frac{\|\Omega^{-1}\|\|\Omega\|}{1-\|\Omega^{-1}\|\|\delta\Omega\|}(\frac{\|\delta\Lambda\|}{\|\Lambda\|}+\frac{\|\delta\Omega\|}{\|\Omega\|})\\ &= \frac{\text{cond}(\Omega)}{1-\text{cond}(\Omega)\frac{\|\delta\Omega\|}{\|\Omega\|}}(\frac{\|\delta\Lambda\|}{\|\Lambda\|}+\frac{\|\delta\Omega\|}{\|\Omega\|})\end{aligned} \tag{19}$$

Eq. (19) gives the upper bound of the relative error coefficient $\frac{\|\delta\boldsymbol{H}\|}{\|\boldsymbol{H}\|}$, and its lower bound is close to zero. Due to the relationship of condition number between the matrix Ω and observation matrix, and that is $\text{cond}(\Omega) = \text{cond}^2(\Psi)$,

we can concentrate on the condition number of the observation matrix. The smaller condition number of the observation matrix is, the more accurate is the joint compliance vector $\boldsymbol{H}$ identified.

Remark 1: In previous studies, dexterity has been used as index to select the robot's joint configurations for joint stiffness identification. However, this classical index focuses on kinematic performance and does not represent other key factors affecting the accuracy of joint stiffness identification. In this paper, as far as we know, it is the first time to propose the relationship between the condition number of the observation matrix and the accuracy of the joint stiffness identification.

B. FINDING SUITABLE POSTURES

The normalized Jacobian matrix can be termed as:

$$J_N = \begin{bmatrix} \frac{1}{L} I_{3\times3} & O_{3\times3} \\ O_{3\times3} & I_{3\times3} \end{bmatrix} J \tag{20}$$

where $I_{3\times3}$ and $O_{3\times3}$ are a 3×3 identity matrix and a 3×3 zero matrix, respectively. L is the characteristic length of the robot, and the Jacobian matrix can be normalized by using this characteristic length [20].

The condition number of the normalized Jacobian matrix J_N based on the Frobenius norm can be termed as [21]:

$$k(J_N) = \frac{1}{6}\sqrt{tr(J_N J_N^T) tr((J_N J_N^T)^{-1})} \tag{21}$$

Dumas *et al.* [13] claimed that the higher the inverse condition number of the normalized Jacobian matrix $k(J_N)^{-1}$ is, the better the dexterity is. Therefore, the condition number of the normalized Jacobian matrix $k(J_N)$ based on the Frobenius norm is used to assess dexterity in this paper. The smaller $k(J_N)$ is, the better the dexterity is.

A novel index to select suitable robot postures for joint stiffness identification has been presented in this paper. This index considers both the dexterity and the condition number of the observation matrix. The detailed steps of postures selection based on it are as follows:

1) Based on the experimental situation, select the suitable bounds of motion of each joint listed in Table 1 to ensure that there is no interference between the robot and other experimental equipment.
2) Select six joint configurations of the robot within the bounds of motion.
3) Assess the dexterity of each posture based on the condition number of the normalized Jacobian matrix $k(J_N)$, and select the maximum value: $k(J_N)_{max} = \max[k(J_N)_i]$ $(i = 1, 2, \cdots, 6)$.
4) Calculate the condition number of the observation matrix cond(Ψ).
5) $k(J_N)_{max} \times$ cond(Ψ) is termed as the novel index, and use the function *fmincon* in MATLAB to find six suitable postures with the smallest value of this index.

Accordingly, the index for suitable postures selection in the joint stiffness identification can be summarized as follows:

TABLE 1. The motion bounds of each joint.

Joint No.	Motion bounds	Joint No.	Motion bounds
1	[-90°, 90°]	4	[-180°, 180°]
2	[-60°, 40°]	5	[-90°, 90°]
3	[-180°, -40°]	6	[-180°, 180°]

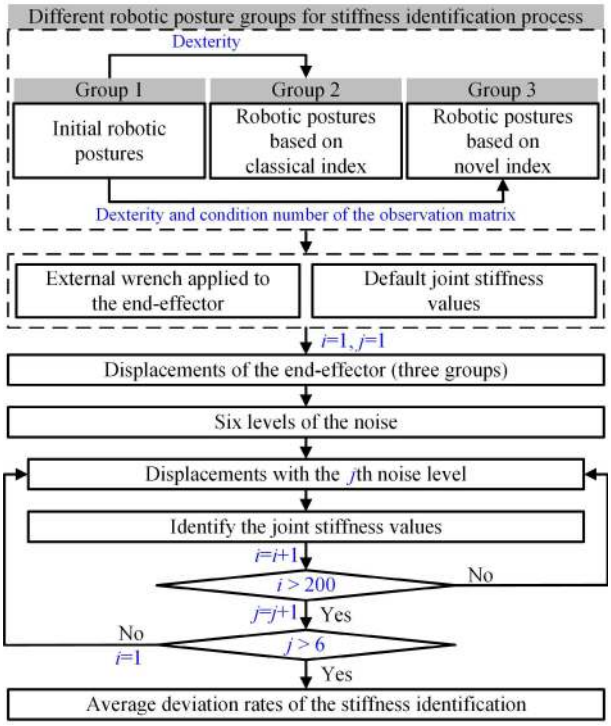

FIGURE 4. Scheme of the numerical simulations.

(1) The classical index considers the dexterity, and that is $k(J_N)_{max}$. The smaller $k(J_N)_{max}$ is, the more suitable postures can be selected. (2) The novel index considers both the dexterity and the condition number of the observation matrix, and that is $k(J_N)_{max} \times$ cond(Ψ). The smaller $k(J_N)_{max} \times$ cond(Ψ) is, the more suitable postures can be selected.

IV. SIMULATIONS AND EXPERIMENTS

A. NUMERICAL SIMULATIONS AND ACCURACY ANALYSIS

To verify the robustness and accuracy of this proposed method for selecting robotic joint configurations based on the novel index, numerical simulations were conducted on MATLAB. In the process, we focus only on the measurement noise generated by the laser tracker. Fig. 4 shows the scheme of the simulations. First, as shown in Fig. 5, six joint configurations of the robot were selected from within its bounds of motion, and this group of postures was called Group 1. This group was used as the initial group of postures for the joint stiffness identification process. Second, the robotic postures were selected based on the classical and novel indices, respectively. Group 2 was selected from Group 1 based on the classical index, and Group 3 was selected from Group 1 based

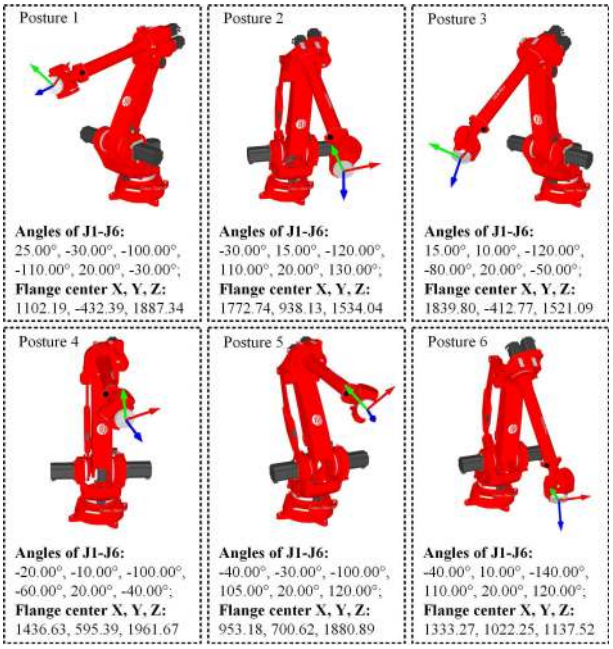

FIGURE 5. Original robotic joint configurations.

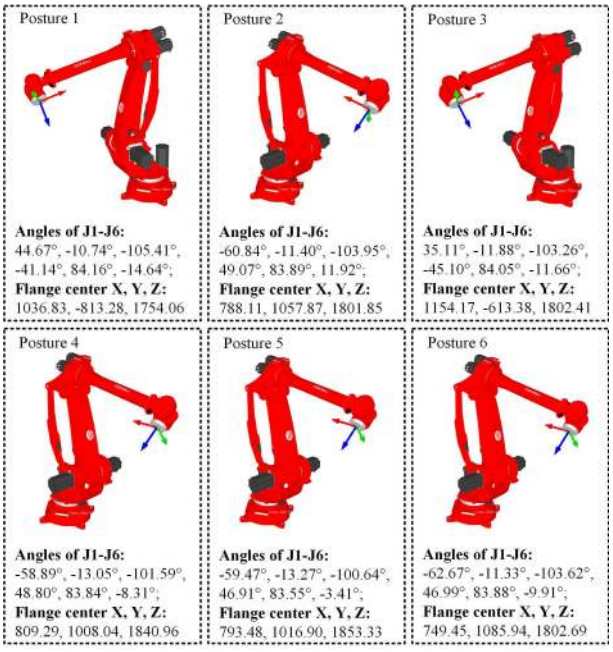

FIGURE 6. Robotic joint configurations based on the classical index.

on the novel index. These two groups of suitable postures are shown in Figs. 6 and 7, respectively. Third, as shown in Table 2, we set the default stiffness values of each joint for the simulations. The precise displacements were calculated when the external wrench was applied to the end-effector, and we focused on the forces and translational displacements. Finally, assuming that the stiffness values of the joints were unknown, we identified them based on translational displacements with the measurement noise. The sensitivity of the

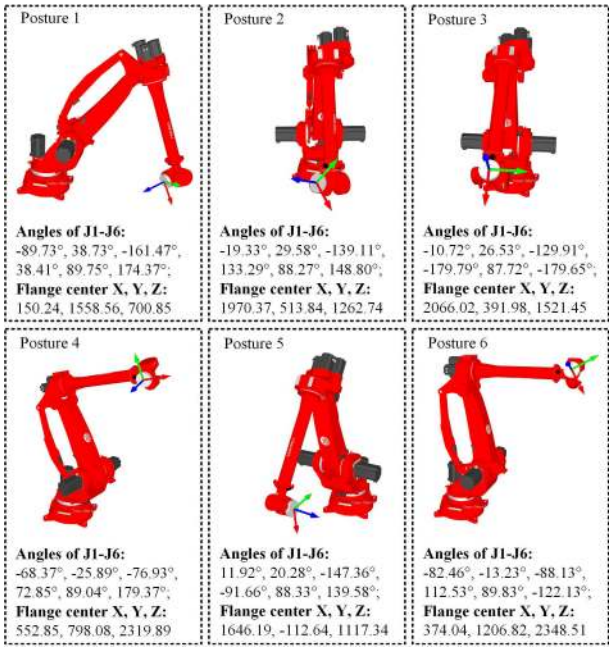

FIGURE 7. Robotic joint configurations based on the novel index.

TABLE 2. Default stiffness values of each joint.

Joint No.	Value (Nm/rad)	Joint No.	Value (Nm/rad)
1	950000	4	250000
2	3000000	5	200000
3	900000	6	150000

results to the measurement noise was analyzed by comparing the identified and the default joint stiffness values.

In the traditional rope–mass loading process, one end of the rope is tied to the loading point of the end-effector and the other to an external loading device. The loading device is used to apply the external wrench on the loading point of the end-effector through the rope. In the base coordinate system of the robot, the position vector of the loading point was calculated based on the robot's posture, which can be termed as:

$$\boldsymbol{P}_1 = [x_1 \quad y_1 \quad z_1]^T$$

The position vector of the other end of the rope tied to the external loading device can be termed as:

$$\boldsymbol{P}_2 = [x_2 \quad y_2 \quad z_2]^T$$

Set G is the external load, and the external force vector $\boldsymbol{F}_{ex} = [f_x \quad f_y \quad f_z]^T$ can be calculated by:

$$\boldsymbol{F}_{ex} = G\frac{\boldsymbol{P}_2 - \boldsymbol{P}_1}{\text{norm}(\boldsymbol{P}_2 - \boldsymbol{P}_1)}$$

Accordingly, the accurate translational displacement vector $[\delta x \quad \delta y \quad \delta z]^T$ can be calculated.

The FARO laser tracker was used in a test to analyze the distribution of the measurement noise. A spherically mounted

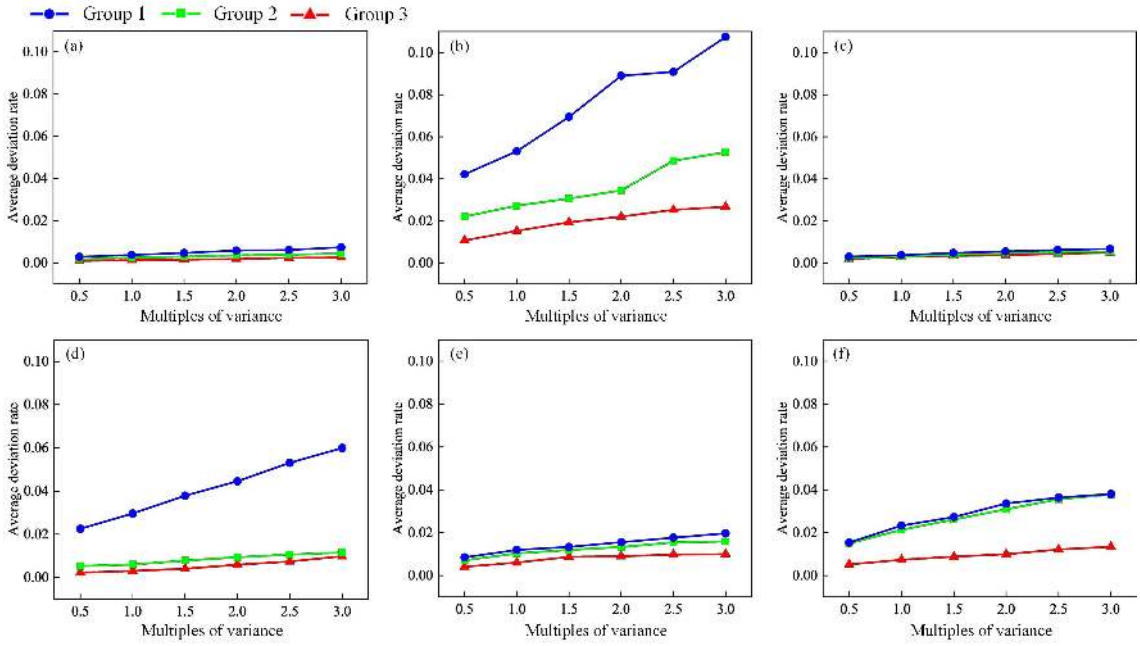

FIGURE 8. Average deviation rates for each joint: (a) the first joint; (b) the second joint; (c) the third joint; (d) the fourth joint; (e) the fifth joint; (f) the sixth joint.

TABLE 3. Multiples of variance of each noise level.

Level	Multiples of variance	Level	Multiples of variance
1	0.5	4	2.0
2	1.0	5	2.5
3	1.5	6	3.0

retroreflector (SMR) was fixed at a point, and the values of each axis were recorded over time. The probability density of the measurement noise was obtained based on the test data, and the variance was $9.23 \times 10^{-5} mm^2$. Therefore, the measurement noise was simulated as white Gaussian noise. With the various multiples of the variance of noise, six levels of measurement noise are listed in Table 3. Let $[\varepsilon_x \quad \varepsilon_y \quad \varepsilon_z]^T$ denote as the measurement noise vector that can be generated by the function *wgn* in MATLAB. Then the translational displacement vector with the noise can be termed as $[\delta x + \varepsilon_x \quad \delta y + \varepsilon_y \quad \delta z + \varepsilon_z]^T$.

A case is provided to illustrate the simulation process for different groups of robot postures at the second noise level:

1) The three groups of robot postures, as shown in Figs. 5-7, were used in the simulation process, respectively.
2) The six diverse robot postures of Group 1 were used one by one. The 500N external load was applied to the loading point of the end-effector. The corresponding displacements of the end-effector were calculated at four measuring points.
3) The noise values were added to the displacements.
4) Steps 2) and 3) were repeated for Groups 2 and 3.

TABLE 4. Deviation rates of each group for the illustration case.

Joint No.	Group 1	Group 2	Group 3
1	0.726%	0.339%	0.268%
2	1.413%	9.845%	0.820%
3	0.251%	0.488%	0.002%
4	7.304%	2.259%	2.075%
5	2.712%	2.236%	0.045%
6	3.242%	2.364%	0.469%

5) The joint stiffness values were identified based on the displacements with noise. The rates of deviation of each group are presented in Table 4.

This case shows that the measurement noise influenced the accuracy of joint stiffness identification for Group 1. Compared with Group 1, Group 2 yielded better identification results, except for the second and third joints. The results for Group 3 were more accurate than those for Group 1.

For each group, 200 simulations were conducted at each noise level, and their average rates of deviation for each joint are shown in Fig. 8. Robustness and accuracy were evaluated based on the average rates of deviation. The lower the average rate of deviation was, the higher the robustness and accuracy of the identification process was. The average rates of deviation of Group 3 were low at different levels of measurement noise. Thus, measurement noise had little influence on the results for this group in the joint stiffness identification process.

B. EXPERIMENTAL WORK

To further verify the robustness and accuracy of the proposed method, experiments on joint stiffness identification were

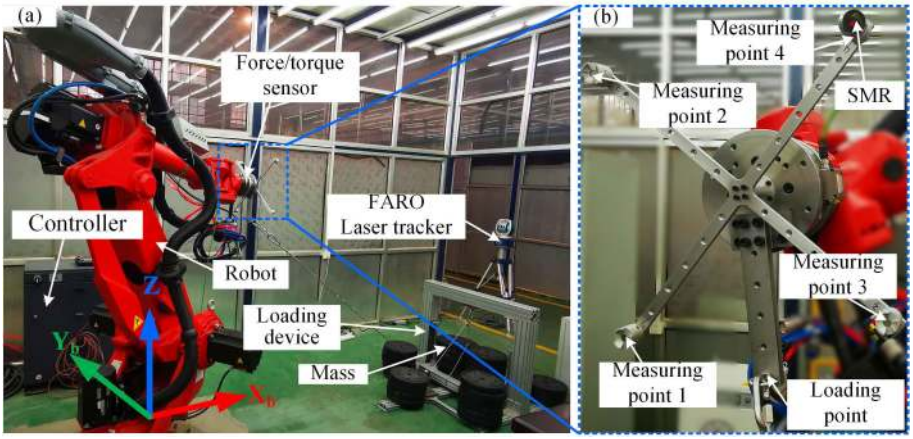

FIGURE 9. The experimental setup for the joint stiffness identification: (a) Schematic of the whole identification system; (b) Schematic of the robot end-effector.

conducted. The experimental system is shown in Fig. 9. The setup included the following parts:

1) The 6 DoFs COMAU SMART5 NJ 165-3.0 industrial robot was used.
2) The six-dimensional ATI force/torque sensor was used to record the force values when the external wrench was applied to the loading point.
3) A special measurement tool with four measuring points and a loading point was attached to the ATI force/torque sensor, and the robot's end-effector consisted of the sensor and the measurement tool.
4) The FARO laser tracker was used to measure the Cartesian coordinates of the four measuring points, along with the SMR.
5) A loading device with several mass blocks (10kg for each one) was used to apply the external load.

A calibration process was carried out before the experiments for the transformation between the robot's base coordinate system and the coordinate system of the laser tracker. The SMR was fixed at measuring point 1, and its center was called the tool center point (TCP). The TCP with reference to the coordinate system of the laser tracker was measured, and its position with reference to the robot's base coordinates was displayed on the teach pendant directly. Five different points were randomly chosen in the robot's workspace and measured by the laser tracker. After each point was measured, the position displayed on the teach pendant was entered into the software; this step was repeated five times.

The FARO laser tracker automatically calculated the transformation matrix for the robot's base coordinate system and its own coordinate system based on the positional information of the five points. In the experiments, this transformation matrix was used in the measurement software. The corresponding measurement process was based on the robot's base coordinate system.

The experiments were conducted in the following steps:

TABLE 5. Three robotic joint configurations for validation.

Joint No.	Posture 1	Posture 2	Posture 3
1	12.81°	-22.25°	-61.35°
2	33.07°	-34.46°	-10.10°
3	-126.36°	-109.53°	-119.99°
4	72.81°	-94.38°	-272.36°
5	-67.88°	49.16°	-55.71°
6	24.27°	186.07°	-110.56°

1) The three robot posture groups, shown in Figs. 5-7, were used in the joint stiffness identification experiments.
2) Six joint configurations from Group 1 were used one by one. The 500N external load was added to the loading device when the robot was in a given posture, and the Cartesian coordinates of the four measuring points were recorded by the FARO laser tracker. The force of the end-effector was measured by the ATI sensor.
3) Step 2) was repeated for Groups 2 and 3, and the corresponding joint stiffness values were identified.
4) The three robot postures listed in Table 5 were used to verify the accuracy of the results of identification. For each posture, 500N external load was applied to the loading point of the end-effector. The accuracy of joint stiffness values was evaluated by comparing the deflections at the four measuring points obtained by calculations and measurements.

The results of joint stiffness identification of the three posture groups are presented in Table 6. The displacements of the end-effector with reference to the measuring points were obtained by both calculations and measurements. The relative translational deflection δb is termed as:

$$\delta b = \sqrt{(\delta x_m - \delta x_c)^2 + (\delta y_m - \delta y_c)^2 + (\delta z_m - \delta z_c)^2} \quad (22)$$

TABLE 6. Results of the joint stiffness identification experiments (Nm/rad).

Joint No.	Group 1	Group 2	Group 3
1	1243000	1516000	852300
2	1704000	5554000	4763000
3	621000	1701000	1312000
4	561000	671000	213000
5	184000	189000	272000
6	413000	102500	173000

TABLE 7. Relative translational deflections of measuring points (mm).

Measuring point No.	Group 1	Group 2	Group 3
1-1	0.558	0.403	0.233
1-2	0.571	0.428	0.192
1-3	0.825	0.449	0.215
1-4	0.868	0.506	0.223
2-1	0.461	0.264	0.168
2-2	0.487	0.302	0.266
2-3	0.519	0.212	0.168
2-4	0.534	0.262	0.206
3-1	0.753	0.628	0.213
3-2	0.737	0.548	0.319
3-3	0.653	0.660	0.253
3-4	0.653	0.590	0.287

* Measuring point No. m-n (m=1, 2, 3, n=1, 2, 3, 4) represents the nth measuring point of the mth posture.

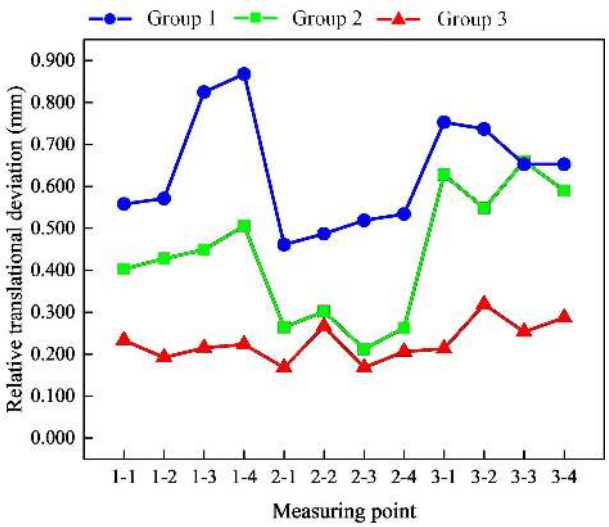

FIGURE 10. The comparison of the relative translational deflections among different posture groups.

where δx_m, δy_m, δz_m and δx_c, δy_c, δz_c represent the measuring and calculating displacements of the X-axis, Y-axis and Z-axis, respectively.

The relative translational deflections of the robot's end-effector with reference to the four measuring points for each posture group are listed in Table 7, and Fig. 10 shows the results of a comparison of the relative translational deflection among the posture groups. The deflection of Group 3 was lower than those of the other groups, and joint stiffness was accurately identified based on the new index.

Remark 2: This paper provides a novel index to select the suitable robot postures in the joint stiffness identification process. Compared with the classical method, the robustness and accuracy of the process of robot postures selection based on this novel index have been verified through the theoretical analysis, simulations and experiments.

V. CONCLUSION

This paper proposed and verified a method to choose the joint configurations of a robot to improve the robustness and accuracy of the process of joint stiffness identification by using a novel index, and presented detailed information about the novel index based on both the dexterity and the condition number of the observation matrix. Simulations and experiments were carried out to verify the robustness and accuracy of the proposed method. The results showed that the joint configurations chosen based on the index developed in this study is more robust and accurate than other solutions. To improve the method in future work, we intend to focus on directly obtaining global optimal joint configurations of the robot.

REFERENCES

[1] S. Mousavi, V. Gagnol, B. C. Bouzgarrou, and P. Ray, "Dynamic modeling and stability prediction in robotic machining," *Int. J. Adv. Manuf. Technol.*, vol. 88, nos. 9–12, pp. 3053–3065, Feb. 2017.

[2] Y. Zhang, K. Guo, and J. Sun, "Investigation on the milling performance of amputating clamping supports for machining with industrial robot," *Int. J. Adv. Manuf. Technol.*, vol. 102, nos. 9–12, pp. 3573–3586, Jun. 2019.

[3] Y. Bu, W. Liao, W. Tian, J. Zhang, and L. Zhang, "Stiffness analysis and optimization in robotic drilling application," *Precis. Eng.*, vol. 49, pp. 388–400, Jul. 2017.

[4] S. Bi and J. Liang, "Robotic drilling system for titanium structures," *Int. J. Adv. Manuf. Technol.*, vol. 54, nos. 5–8, pp. 767–774, May 2011.

[5] Y. Guo, H. Dong, G. Wang, and Y. Ke, "Vibration analysis and suppression in robotic boring process," *Int. J. Mach. Tools Manuf.*, vol. 101, pp. 102–110, Feb. 2016.

[6] D. Deblaise, X. Hernot, and P. Maurine, "A systematic analytical method for PKM stiffness matrix calculation," in *Proc. IEEE Int. Conf. Robot. Autom.*, Dec. 2006, pp. 4213–4219.

[7] G. Ibrahimcan, C. Giuseppe, and I. C. D. Mehmet, "Time efficient stiffness model computation for a parallel haptic mechanism via the virtual joint method," *Mech. Mach. Theory*, vol. 103614, pp. 58–71, Dec. 2020.

[8] J. Salisbury, "Active stiffness control of a manipulator in Cartesian coordinates," in *Proc. 19th IEEE Conf. Decis. Control including Symp. Adapt. Processes*, Dec. 1980, pp. 87–97.

[9] S.-F. Chen and I. Kao, "Conservative congruence transformation for joint and Cartesian stiffness matrices of robotic hands and fingers," *Int. J. Robot. Res.*, vol. 19, no. 9, pp. 835–847, Sep. 2000.

[10] E. Abele, M. Weigold, and S. Rothenbächer, "Modeling and identification of an industrial robot for machining applications," *CIRP Ann.*, vol. 56, no. 1, pp. 387–390, 2007.

[11] C. Dumas, S. Caro, M. Cheírif, S. Garnier, and B. Furet, "A methodology for joint stiffness identification of serial robots," in *Proc. IEEE/RSJ Int. Conf. Intell. Robots Syst.*, Oct. 2010, pp. 464–469.

[12] Y. Guo, H. Dong, and Y. Ke, "Stiffness-oriented posture optimization in robotic machining applications," *Robot. Comput.-Integr. Manuf.*, vol. 35, pp. 69–76, Oct. 2015.

[13] C. Dumas, S. Caro, S. Garnier, and B. Furet, "Joint stiffness identification of six-revolute industrial serial robots," *Robot. Comput.-Integr. Manuf.*, vol. 27, no. 4, pp. 881–888, Aug. 2011.

[14] K. Yang, W. Yang, G. Cheng, and B. Lu, "A new methodology for joint stiffness identification of heavy duty industrial robots with the counterbalancing system," *Robot. Comput.-Integr. Manuf.*, vol. 53, pp. 58–71, Oct. 2018.
[15] L. Cen and S. N. Melkote, "CCT-based mode coupling chatter avoidance in robotic milling," *J. Manuf. Processes*, vol. 29, pp. 50–61, Oct. 2017.
[16] G. Alici and B. Shirinzadeh, "Enhanced stiffness modeling, identification and characterization for robot manipulators," *IEEE Trans. Robot.*, vol. 21, no. 4, pp. 554–564, Aug. 2005.
[17] C. Lehmann, B. Olofsson, K. Nilsson, M. Halbauer, M. Haage, A. Robertsson, O. Sörnmo, and U. Berger, "Robot joint modeling and parameter identification using the clamping method," *IFAC Proc. Volumes*, vol. 46, no. 9, pp. 813–818, 2013.
[18] D. J. Bennett, J. M. Hollerbach, and P. D. Henri, "Kinematic calibration by direct estimation of the jacobian matrix," in *Proc. IEEE Int. Conf. Robot. Autom.*, Jan. 1992, pp. 351–352.
[19] A. Jubien, G. Abba, and M. Gautier, "Joint stiffness identification of a heavy kuka robot with a low-cost clamped end-effector procedure," in *Proc. 11th Int. Conf. Informat. Control, Autom. Robot.*, 2014, pp. 585–591.
[20] B. Paden and S. Sastry, "Optimal kinematic design of 6R manipulators," *Int. J. Robot. Res.*, vol. 7, no. 2, pp. 43–61, Apr. 1988.
[21] G. Golub and C. Van Loan, *Matrix Computations*, 3rd ed. Baltimore, MD, USA: Johns Hopkins University Press, 1996.

YIRAN ZHANG received the B.S. degree in mechanical design and automation engineering from the North University of China, Taiyuan, China, in 2016. He is currently pursuing the Ph.D. degree in mechanical engineering with Shandong University, Jinan, China.

His current research interests include machining with industrial robot, chatter suppression, and manufacturing process monitoring.

KAI GUO (Member, IEEE) received the Ph.D. degree in fluid power transmission and control from Zhejiang University, Hangzhou, China, in 2015.

He is currently an Associate Professor with the Key Laboratory of High Efficiency and Clean Mechanical Manufacture of Ministry of Education, Department of Mechanical Engineering, Shandong University, China. His current research interests include the intelligent manufacturing, robot dynamics, and nonlinear control systems.

JIE SUN received the Ph.D. degree in mechanical engineering from Zhejiang University, Hangzhou, China, in 2004.

He is currently a Professor with the School of Mechanical Engineering, Shandong University, Jinan, China. His current research interests include the high speed cutting mechanism of difficult-to-machine materials, deformation control and correction of NC machining of large structure components, intelligent manufacturing, laser processing, and remanufacturing.

YUJING SUN received the Ph.D. degree from Shandong University, Jinan, China, in 2014.

From September 2011 to September 2012, she was a Visiting Scholar with Clemson University, USA. She is currently a Lecturer with the Qilu University of Technology, Jinan. Her current research interests include the machining of difficult-to-cut materials and intelligent manufacturing.